Purdue University
Purdue e-Pubs

International Refrigeration and Air Conditioning Conference

School of Mechanical Engineering

2010

Numerical Assessment of Frosting and Defrosting of 'No-Frost' Evaporators

Fernando Knabben
Federal University of Santa Catarina

Christian Hermes
Federal University of Parana

Claudio Melo
Federal University of Santa Catarina

Follow this and additional works at: http://docs.lib.purdue.edu/iracc

Knabben, Fernando; Hermes, Christian; and Melo, Claudio, "Numerical Assessment of Frosting and Defrosting of 'No-Frost' Evaporators" (2010). *International Refrigeration and Air Conditioning Conference.* Paper 1014.
http://docs.lib.purdue.edu/iracc/1014

This document has been made available through Purdue e-Pubs, a service of the Purdue University Libraries. Please contact epubs@purdue.edu for additional information.
Complete proceedings may be acquired in print and on CD-ROM directly from the Ray W. Herrick Laboratories at https://engineering.purdue.edu/Herrick/Events/orderlit.html

Numerical Assessment of Frosting and Defrosting of 'No-Frost' Evaporators

Fernando T. KNABBEN [1], Christian J. L. HERMES [2*], Cláudio MELO [1]

[1] POLO Research Laboratories for Emerging Technologies in Cooling and Thermophysics,
Department of Mechanical Engineering, Federal University of Santa Catarina
88040-970, Florianópolis, SC, BRAZIL

[2] Department of Mechanical Engineering, Federal University of Paraná,
P.O. Box 19011, 81531-990, Curitiba, PR, BRAZIL

[*] Corresponding Author, Phone: ++55 41 3361 3239, e-mail: chermes@ufpr.br

ABSTRACT

This paper presents a numerical study on the frosting and defrosting processes in 'no-frost' evaporators, a type of heat exchanger typically found in household refrigerators. A two-dimensional numerical model, based on mass and energy balances within the frost layer, was developed to predict the time variation in the frost thickness, and also the heat and mass transfer rates. The model takes into account the hydrodynamic coupling between the fan and the frosted coil, in such a way as to predict the airflow changes due to progressive evaporator blockage. The model predictions for pressure drop and frost mass were compared with experimental data taken under different operating conditions (cabinet air temperature and relative humidity, and coil surface temperature), and a reasonable level of agreement was achieved, with all predictions falling within a ±10% error band. The model was then used to assess the impact of several design parameters (including fin pitch and distribution, and defrost heater power and distribution) on both the evaporator blockage and defrosting efficiency. It was found that an almost ideal defrosting efficiency is achieved when the process is carried out by two simultaneous heaters, one for the first 6 rows and another for the last 4 rows.

1. INTRODUCTION

In several engineering applications, such as aerospace, refrigeration and food preservation, frost is undesirable since it has a negative impact on equipment performance (e.g., frost clogging of refrigeration evaporators) and safety (e.g., frost accumulation on aircraft wings). The cooling capacity of refrigeration systems is depleted by evaporator frosting because the frost layer adds an extra thermal resistance to the heat transfer process and also because it increases the air pressure drop, thereby substantially reducing the fan-supplied airflow rate. As a consequence, the temperatures of the refrigerated compartments go up and the compressor runtime increases. The frost accumulated on the evaporator coil must thus be periodically removed, usually by electrical heaters. As the energy consumption targets for household refrigeration appliances are constantly being lowered by Government actions worldwide, efforts are being made by manufacturers to gain a better understanding of the frosting and defrosting processes of evaporator coils.

In spite of the large amount of publications in this field, few authors have actually studied the frost accumulation on 'no-frost' evaporators (Ogawa *et al*., 1993; Inan *et al.,* 2002; Seker *et al*., 2004a,b; Ozkan *et al*., 2006; Yang *et al*., 2006). Moreover, most of these have investigated this phenomenon with the aid of a wind-tunnel test facility, where the velocity, temperature and humidity of the air stream at the evaporator inlet were kept constant during the tests. This constraint is unlikely to be found in real 'frost-free' refrigerators, where the warm and humid air stream from the fresh-food compartment is cooled down in the central part of the evaporator, and the cold and dry air stream from the freezer compartment passes through the right and left ends, as illustrated in Fig. 1. It is worth mentioning that none of the previous studies have considered the effect of frost on the fan-supplied airflow rate and evaporator effectiveness. Furthermore, there is no evidence that the impact of the defrost strategy on the defrost efficiency was investigated by any of the previous studies.

The aim of this study is to cover some of the lacunas left by the previous investigators, by developing a numerical 2-D model to study the frosting and defrosting processes in 'no-frost' evaporators. Such a model predicts the heat and mass transfer rates of the evaporator coil and takes into account the effect of the frost layer on the air pressure drop and consequently on the fan-supplied air flow rate.

2. FROST FORMATION MODEL

The modeling strategy adopted in this study is essentially that proposed by Knabben *et al*. (2010), who divided the mathematical model into three sub-models, namely the air flow model, heat exchanger model, and frost growth model. The first calculates the amount of air flowing into each region of the evaporator (see Fig. 1), the second the heat and mass transfer rates to the frost layer, and the third the frost thickness growth over time. In 'no-frost' refrigerators, there are two air streams returning to the evaporator: warm humid air from the fresh-food compartment, flowing through the central part of the evaporator, and cold dry air from the freezer compartment, flowing through the left and right ends of the evaporator (see Fig. 1). Therefore, in order to account for the non-uniform boundary conditions (air flow rate, temperature, humidity) at the evaporator inlet, the evaporator was discretized into 30 control volumes, with 10 along the length and 3 along the width. It is worth mentioning that only 20 control volumes were actually implemented due to the symmetry of the left and right side air flows.

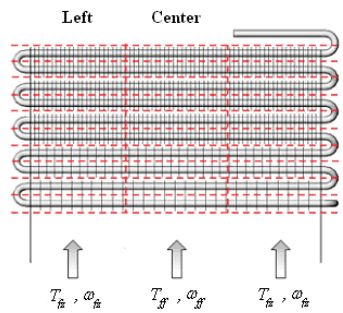

Figure 1. Two-dimensional mesh of the 'no-frost' evaporator

Since the levels of the air pressure drops in the left, right and central control volumes, situated at the same position along the length, must be the same, the air flow rate through each region needs to be adjusted to obey the momentum equation. Figure 2 illustrates a situation where the air pressure drops at the left and right side control volumes are higher than that at the center. Thus, part of the air flow is moved from the sides to the center. In contrast, when the pressure drop at the center is higher than those at the sides, air is moved in the opposite direction. Mathematically, when $\Delta P_l > \Delta P_c$, the air flow is directed toward the center, yielding

$$(\rho V)_{l,cv} = (\rho V)_l (1 - r) \tag{1}$$

$$(\rho V)_{c,cv} = (\rho V)_c + 2(\rho V)_l r \tag{2}$$

where r is the iteratively calculated fraction of air deviated from the lateral to the central control volume. The supplied air flow rate is calculated by simultaneously solving the characteristic equations for the fan and air distribution system, the latter being expressed as

$$\Delta P = \Delta P_{4-3} = K_{4-1}\rho V^2 + \Delta P_{1-2} + K_{2-3}\rho V^2 \tag{3}$$

where the coefficients $K_{4\text{-}1}$ and $K_{2\text{-}3}$ were obtained previously with the aid of a wind-tunnel test facility (Barbosa *et al*., 2009). The airside pressure drop through the evaporator was calculated by the correlation proposed by Barbosa *et al.* (2009). The characteristic equation for the fan was expressed as a third-order polynomial fit. A heat exchanger model is needed to evaluate the energy and mass transfer rates to the frost layer. To this end, the following generic differential equation was derived, based on mass and energy balances at the frost layer surface:

$$\frac{\mathrm{d}y}{\mathrm{d}A_s} = h\eta_s (\rho V_{cv} c_p L)^{-1} (y_s - y) \tag{4}$$

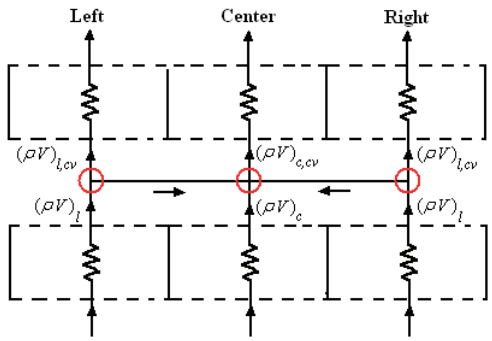

Figure 2. Air flow distribution among the control volumes

where $y=\omega$ and $L=\mathrm{Le}^{2/3}$ relate to the mass conservation equation, and $y=T$ and $L=1$ to the sensible energy conservation equation. Assuming that y_s, $h\eta_s$ and $\rho V_{cv}c_p$ are constant at each control volume, equation (4) can be analytically integrated, yielding

$$y_o = y_s + (y_s - y_i)\exp\left[-h\eta_s A_s \left(\rho V_{cv} c_p L\right)^{-1}\right] \tag{5}$$

where $A_s=A_t+A_{fin}$ is the frost surface area, and $h\eta_s$ is calculated from the correlation proposed by Barbosa *et al.* (2009). Equation (5) provides the temperature and absolute humidity downstream of each control volume, and the sensible and latent heat transfer rates, respectively, are calculated from:

$$Q_{sen} = \rho V_{cv} c_p (T_i - T_o) \tag{6}$$

$$Q_{lat} = \rho V_{cv} (\omega_i - \omega_o) i_{sv} \tag{7}$$

The frost growth process was modeled based on the work of Hermes *et al.* (2009), bearing in mind the following simplifying assumptions: (i) the mass and energy transport within the frost layer is purely diffusive, quasi-steady and one-dimensional; (ii) the frost layer thickness is uniform and has an isothermal surface; (iii) the coil surface temperature is uniform and equal to the evaporation temperature; and (iv) the Lewis analogy applies. The model splits the total mass flux into two terms, namely growth and densification, yielding

$$m = m_g + m_d = \rho_f \frac{\mathrm{d}x_f}{\mathrm{d}t} + x_f \frac{\mathrm{d}\rho_f}{\mathrm{d}t} = \frac{\rho V_{cv}}{A_s}(\omega_i - \omega_o) \tag{8}$$

Assuming that the frost density variation with time is negligible, the densification mass flux was considered nil. The frost density was assumed to be uniform and was calculated, as proposed by Knabben *et al.* (2010), as

$$\rho_f = 492.95\exp\left[-0.053\left(T_{dew,ff} - T_e\right)\right] \tag{9}$$

The frost surface temperature and humidity, which are input data for the heat exchanger model, were obtained by solving the equations for the mass and energy diffusion within the porous media (Hermes *et al.*, 2009), yielding

$$T_s = T_e + \frac{Q}{A_s}\frac{x_f}{k_f} - \frac{\rho\omega_{sat,e} i_{sv}}{k_f}\frac{D\varepsilon}{\tau}\left[cosh\left(\frac{\omega_{sat,s}}{\omega_{sat,e}}\right) - 1\right] \tag{10}$$

$$\omega_s = \omega_{sat,s} = \omega_{sat,e}\, cosh\left(\sqrt{\lambda\tau\varepsilon^{-1}D^{-1}x_f^2}\right) \tag{11}$$

The frost thickness and the frost mass on the evaporator surface at each time step are calculated through a first-order explicit integration scheme, as follows:

$$x_f^{t+\Delta t} = x_f^t + \left(m^t / \rho_f^t\right)\Delta t \tag{12}$$

$$M^{t+\Delta t} = M^t + \left(m^t A_s^t\right)\Delta t \tag{13}$$

Figure 3 compares the numerical predictions for the pressure drop and the frost mass with the experimental data collected by Knabben *et al.* (2010). It may be seen that a satisfactory level of agreement between the calculated and measured counterparts is achieved, with all predictions falling within a ±10% error band. Moreover, it can also be noted that the model follows closely the experimental trends.

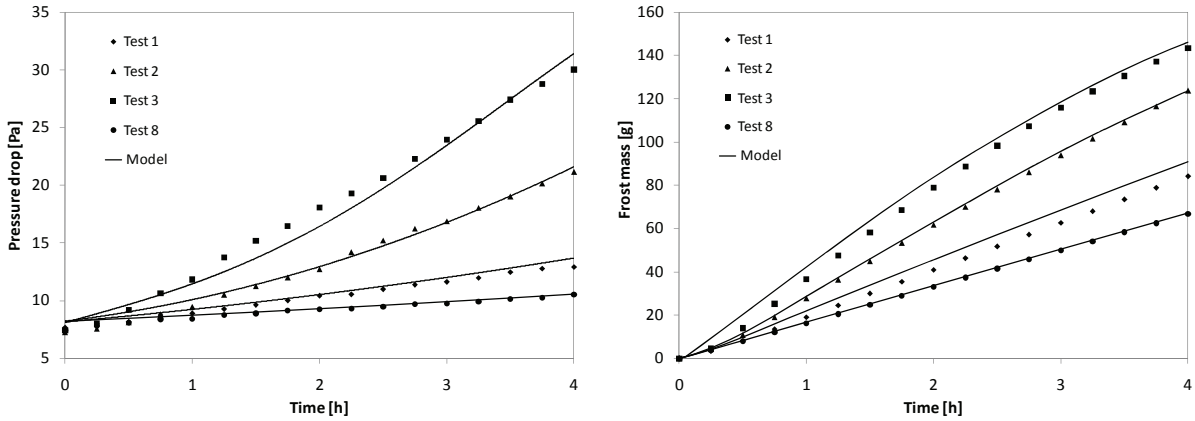

Figure 3. Predicted versus measured pressure drop (left) and frost mass (right)

3. NUMERICAL ASSESSMENT

The following numerical analysis was carried out assuming that the central air stream is at 4.7ºC and 80.5% relative humidity, the lateral air streams are at -15.2ºC, and the evaporator coil is at -23.3ºC. This set of conditions is typically found in household refrigerators (Knabben *et al.*, 2010). Moreover, it was assumed that the defrosting process is carried out by a 235W defrost heater uniformly distributed along the evaporator.

3.1 Fin spacing and distribution

This analysis was carried out by varying the number of evaporator fins, and subsequently the fin spacing, as shown in Table 1. It should be noted that these modifications were introduced not only to decrease the number of fins in the outlet region of the evaporator (where the temperature and humidity differences between the frost surface and the air stream are low) but also to avoid the evaporator blockage in the regions where the percentage free flow area is rather small (for instance, between rows 4 and 5). Figures 4 and 5 show the percentage free flow area and the time variation of the frost mass and cooling capacity for all the alternatives presented in Table 1, respectively.

Table 1: Proposed alternatives for fin spacing

Setup	Rows 1 / 2	Rows 3 / 4	Rows 5 / 6	Rows 7 / 8	Rows 9 / 10
Original	26	34	67	67	67
Alternative 1	26	34	42	67	67
Alternative 2	26	34	42	42	67
Alternative 3	26	26	34	42	42

Figure 5 shows that the cooling capacity of the original evaporator drops sharply after 3.5 hours, due to the partial blockage of row 5. This behavior is not observed with alternative 1 where 25 fins were removed from row 5, thereby increasing the percentage free flow area for this row after 4 hours, from 6% (original) to 15%. As a drawback the cooling capacity of alternative 1 was 2.5% lower during most of the transient time. The second proposed configuration was to remove another 25 fins, this time from row 7 (alternative 2), and this increased the percentage free flow for this row after 4 hours, from 26% (original) to 33% with a maximum penalty of 4.5% in terms of cooling capacity. The third proposed configuration was to remove a further 8 fins from both rows 3 and 5 (alternative 3). In this case the percentage free flow area for row 3 after 4 hours increased from 6% (original) to 13% with a maximum penalty of 10% in terms of cooling capacity.

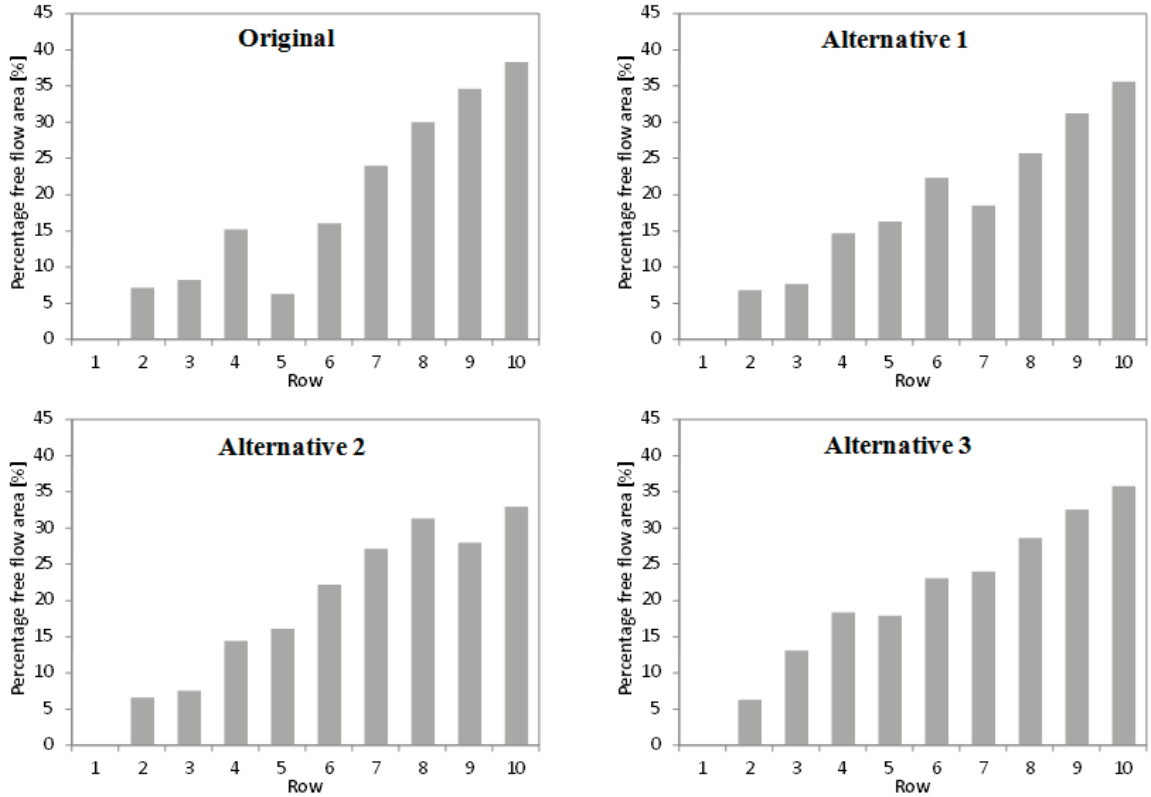

Figure 4. Percentage free flow area in the central region of the evaporator

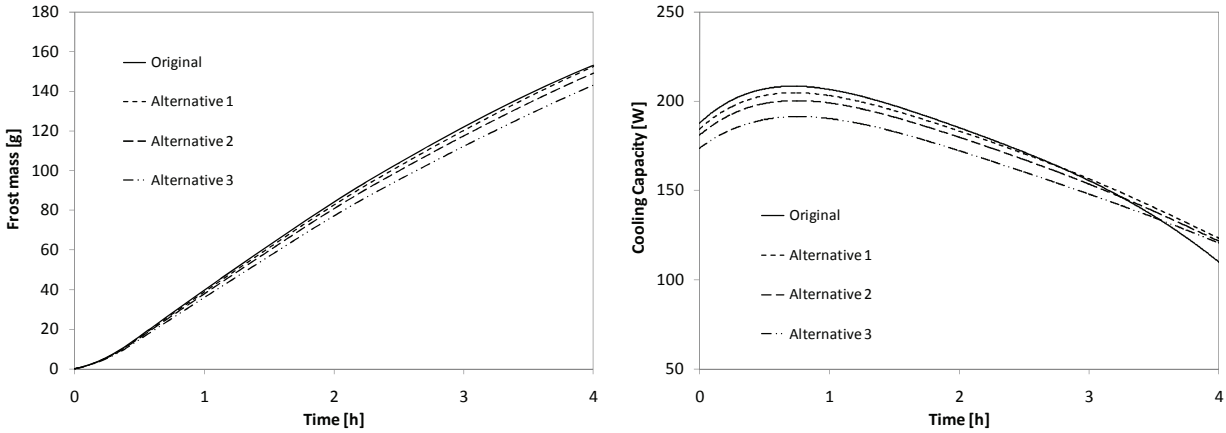

Figure 5. Reduction in frost mass (left) and cooling capacity (right) for different numbers of fins

3.2 Fan-supplied air flow rate

The impact of the air flow rate on the frost accumulation was assessed by varying the fan speed. The characteristic curves of the fan at other speeds were constructed using the fundamental fan laws. The cooling capacity is known to be a direct function of the fan speed, as is the frost accumulation rate (see Fig. 6). Therefore there is a trade-off between cooling capacity and evaporator blockage that has to be considered when choosing the fan speed for a certain application.

3.3 Defrosting strategy

In order to consider different defrosting strategies an estimate of the frost distribution over the evaporator coil is required. Figure 7 shows the frost distribution predicted by the model, according to the tube row and flow region. It can be observed that the frost accumulates mostly along the first central rows where the humidity gradients are higher than in the other regions. It can also be noted that the frost accumulation tends to decrease along the

evaporator length, with the exception of row 5, where the finned surface is much higher than that of the previous row.

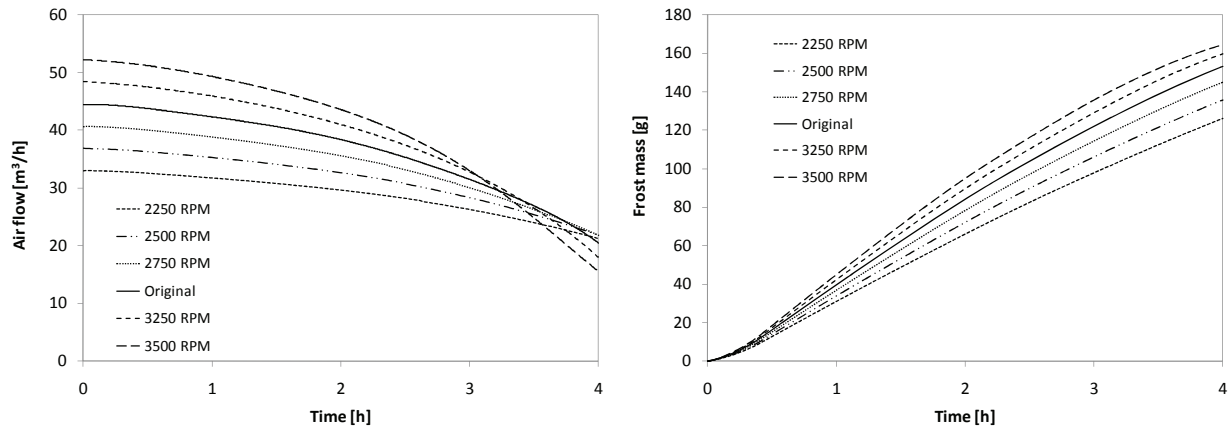

Figure 6. Air flow rate (left) and frost mass (right) as a function of time for different fan speeds

Table 2 shows the percentage of the heater power that should be dissipated along each tube row to remove the accumulated frost mass. It is worth mentioning that if the power is ideally distributed the defrosting efficiency will be unitary. With such a distribution and with a 235 W electrical heater, the defrosting process would take approximately 3.67 minutes, less than half the time actually required (8.5 minutes). Alternatively, if the defrosting time is kept at 8.5 min, the amount of power needed would drop to 100 W.

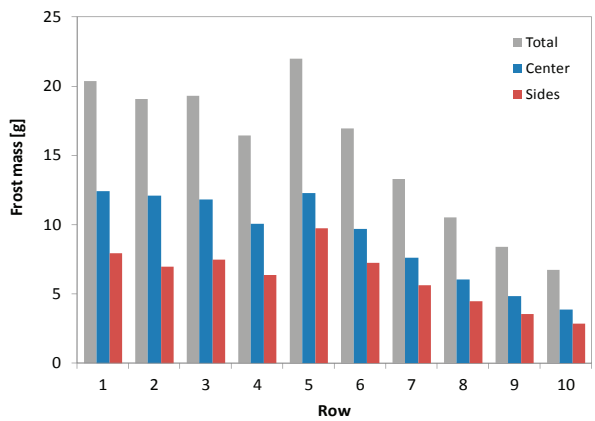

Figure 7. Frost mass distribution among the evaporator rows

However, the non-uniform distribution of the heater power indicated in Table 2 is not practical. An alternative would be to split the total heater power into two values, 75% (175W) for the first 6 rows and 25% (60W) for the last four rows. This alternative for the defrosting process would take approximately 3.67 minutes and the defrost efficiency would be very close to that obtained ideally (see Table 3).

Table 2: Percentage heater power for each evaporator row

Row	1	2	3	4	5	6	7	8	9	10
Heater power [%]	13.3	12.5	12.6	10.7	14.4	11.1	8.7	6.9	5.5	4.4

Table 3: Proposed heat distribution

Row	1	2	3	4	5	6	7	8	9	10
Ideal [W]	31.2	29.2	29.6	25.2	33.8	26.0	20.4	16.2	12.9	10.3
Alternative [W]	29.2	29.2	29.2	29.2	29.2	29.2	15.0	15.0	15.0	15.0
Difference [%]	2.1	0.1	0.4	-3.9	4.6	-3.1	5.4	1.2	-2.1	-4.7

4. CONCLUDING REMARKS

An assessment of the impact of several design parameters on the performance of 'no-frost' evaporators, such as fin spacing, fan-supplied air flow rate, and defrosting strategy was carried out numerically using a two-dimensional simulation model that accounts for the frost accretion on the evaporator coil. It was observed that the addition of fins between rows 4 and 5 may induce local evaporator blockage. It was also shown that there is a trade-off between cooling capacity and frost accumulation as the fan speed increases. A numerical mapping of the frost mass distribution over the evaporator coil was also carried out. It was found that defrosting efficiencies close to unity would be reached if the defrosting process is carried out by the simultaneous action of two heaters, one of 175W for the 6 first rows and another of 60 W for the last four rows.

ACKNOWLEDGEMENTS

This study was carried out at the POLO Labs facilities under National Grant No. 573581/2008-8 (National Institute of Science and Technology in Refrigeration and Thermophysics) funded by the CNPq Agency. Technical support from Whirlpool S.A. is also duly acknowledged.

REFERENCES

Barbosa, J.R., Melo, C., Hermes, C.J.L., Waltrich, P.J., 2009, A Study of the Air-Side Heat Transfer and Pressure Drop Characteristics of Tube-Fin No-Frost Evaporators, *Applied Energy*, vol. 86(9), p. 1484-1491.

Hermes, C.J.L., Piucco, R.O., Barbosa, J.R., Melo, C., 2009, A study of frost growth and densification on flat surfaces, *Experimental Thermal and Fluid Science*, vol. 33(2), p. 371-379.

Inan, C., Karatas, H., Egrican, N., Lale, C., 2002, Real time upright freezer evaporator performance under frosted conditions, *International Refrigeration and Air Conditioning Conference at Purdue*, West Lafayette, IN, USA.

Knabben, F.T., Hermes, C.J.L., Melo, C., 2010, An in-situ study of frost accretion on no-frost evaporators, *ASME-ATI-UIT 2010 Conference on Thermal and Environmental Issues in Energy Systems*, Sorrento, Italy.

Ogawa, K., Tanaka, N., Takeshita, M., 1993, Performance improvement of plate fin-and-tube heat exchangers under frosting conditions, *ASHRAE Transactions*, vol. 99, p. 762-771.

Ozkan, D.B., Ozil, E., 2006, Experimental study on the effect of frost parameters on domestic refrigerator finned tube evaporator coils, Applied Thermal Engineering, vol. 26(17), p. 2490-2493.

Seker, D., Karatas, H., Egrican, N., 2004a, Frost formation on fin-and-tube heat exchangers, Part I – Modeling of frost formation on fin-and-tube heat exchangers, *Int. J. of Refrigeration*, vol. 27, p. 367-374.

Seker, D., Karatas, H., Egrican, N., 2004b, Frost formation on fin-and-tube heat exchangers. Part II – Experimental investigation of frost formation on fin-and-tube heat exchangers, *Int. J. of Refrigeration*, vol. 27, p. 375-377.

Yang, D.K., Lee, K.S., Song, S., 2006, Modeling for predicting frosting behavior of a fin–tube heat exchanger, *International Journal of Heat and Mass Transfer*, vol. 49(7), p. 1472-1479.

NOMENCLATURE

D	diffusivity of water vapor in air, $m^2\ s^{-1}$
f	friction factor
h	convection heat transfer coefficient, $W\ m^{-2}\ K^{-1}$
i_{sv}	latent heat of desublimation, $J\ kg^{-1}$
k	thermal conductivity, $W\ m^{-1}\ K^{-1}$
V	air flow rate, $m^3\ s^{-1}$
α	thermal diffusivity, $m^2\ s^{-1}$
ε	porosity
η	surface effectiveness of the heat exchanger
ϕ	relative humidity
λ	desublimation coefficient, s^{-1}
ρ	density, $kg\ m^{-3}$
τ	tortuosity
ω	humidity ratio, $kg_v\ kg_a^{-1}$

Subscripts

c	central region of the evaporator
cv	control volume
d	densification
dew	dew point
e	evaporating temperature
f	frost
ff	fresh-food
fz	freezer
g	growth
i	inlet
l	lateral regions of the evaporator
o	outlet
s	frost surface